Inorganic Chemistry

pubs.acs.org/IC Article

Sulfide Oxidation by 2,6-Bis[hydroxyl(methyl)amino]-4-morpholino-1,3,5-triazinatodioxomolybdenum(VI): Mechanistic Implications with DFT Calculations for a New Class of Molybdenum(VI) Complex

Cayden X. Bullock, Cooper S. Jamieson, Pierre Moënne-Loccoz, Buck Taylor, Jordan A. M. Gonzalez, Ellie A. Draves, and Louis Y. Kuo*

Cite This: *Inorg. Chem.* 2021, 60, 7762–7772 Read Online

ACCESS | Metrics & More | Article Recommendations | Supporting Information

ABSTRACT: Sulfide oxidation is accomplished by a new class of dioxomolybdenum(VI) catalyst (**1**) that uses the tridentate 2,6-bis[hydroxyl(methyl)amino]-4-morpholino-1,3,5-triazine ligand to form a five-coordinate molybdenum(VI) center. Resonance Raman spectra show that the dioxo groups on the Mo(VI) oxygens readily exchange with water in an acetonitrile media that allows ^{18}O labeling of catalyst **1**. The model oxidation reaction was the conversion of thioanisole (**2**) to the corresponding sulfoxide with 4% of **1** using an equimolar amount of H_2O_2 in MeCN-d_3. Oxygen-18 labeling experiments with either ^{18}O-labeled **1** or ^{18}O-labeled H_2O_2 are consistent with a sulfide oxygenation pathway that uses a η^1-Mo(OOH) hydroxoperoxyl species (**3**). The hypothesized intermediate **3** is initially formed in a proton transfer reaction between **1** and H_2O_2. Oxidation is hypothesized via nucleophilic attack of the sulfide on **3** that is supported from a Hammett linear free-energy relationship for para-derivatives of **2**. A Hammett reactivity constant (ρ) of -1.2 ± 0.2 was obtained, which is consistent with other ρ values found in prior sulfide oxidation reactions by group 6 complexes. An Eyring plot of the **2** oxidation by **1** gives an E_a of 63.0 ± 5.2 kJ/mol, which is slightly higher than that of a similar oxidation of **2** by the molybdenum(VI) complex, oxodiperoxo (pyridine-2-carboxylato)molybdate(VI) bis(pyridine-2-carboxylic acid) monohydrate (**5**). Computational modeling with density functional theory (DFT) of the complete reaction profile gave enthalpy and entropy of activations (64 kJ/mol and −120 J/mol·K, respectively) within 1 standard deviation of the experimental values, further supporting the hypothesized mechanism.

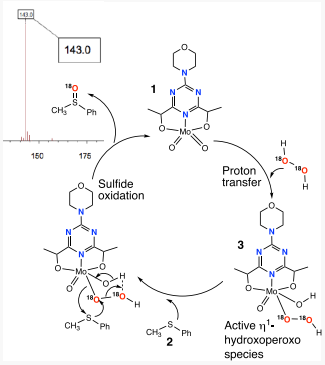

INTRODUCTION

Fossil fuel combustion, which is the mainstay energy source for the immediate future,[1] inevitably yields SO_x emissions.[2] Such sulfur emissions lead to environmental pollutions such as acid rain and smog.[3] As such, environmental regulations have mandated a maximum sulfur content of 10 ppm in fuels,[4] and this has led to the production of clean fossil fuels with low sulfur contents. Hydrodesulfurization (HDS) is the main method for removing sulfur such as mercaptans, sulfides, and disulfides from fossil fuels.[5] Among alternate protocols is oxidative desulfurization (ODS), which has the advantages of its low cost and mild reaction conditions;[6] HDS requires high temperature and high H_2(g) pressure. The strategy behind ODS is the creation of a polar sulfoxide and/or sulfone that readily separates from the hydrocarbon for sulfur removal (eq 1)

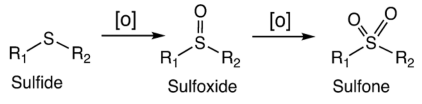

(1)

Hydrogen peroxide[7] is still the oxidant of choice for ODS but activation of H_2O_2 requires an appropriate catalyst. To that end, a number of molybdenum(VI) complexes have been developed as ODS catalysts and they include both polyoxomolybdates of the forms $[\{MoO(O_2)_2\}_2(\mu\text{-}O)]^{2-}$[8] and lanthanopolyoxo-molybdate[9] and alkylimidazolium[10] octamolybdate as well as mononuclear coordination Mo(VI) peroxo complexes.[11] In terms of this set of Mo(VI) compounds, we were interested in using discrete $Mo(=O)_2$ dioxo complexes as possible sulfide oxidation catalysts. The strategy uses the dioxo form as a stable precatalyst, which, upon activation by peroxide, is converted to the active Mo(OO) peroxo complex that carries out sulfide oxidation. To that end, we report that stabilization of the $Mo(=O)_2$ dioxo functionality by the ligand 2,6-bis[hydroxy(methyl)amino]-4-morpholino-1,3,5-triazine (H_2bihyat)[12] yields a catalyst that effectively oxidizes model sulfides. This compact pincer ligand was utilized by Kabanos and co-workers to chelate a variety of high oxidation, hard metal ions (Mo(VI), V(V), Fe(III))[13] including uranium-(VI).[14] Recently, the H_2bihyat system was grafted to a

Received: January 17, 2021
Published: May 13, 2021

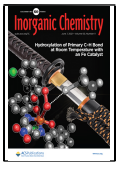

https://doi.org/10.1021/acs.inorgchem.1c00145
Inorg. Chem. 2021, 60, 7762–7772

polyethylene support to selectively bind UO^{2+}.[15] We report the first case of utilizing this chelator for the catalytic oxidation of model alkyl sulfides selectively to the corresponding sulfoxide. The previously known complex {2,6-bis[hydroxy(methyl)-amino]-4-morpholino-1,3,5-triazinato-O,N,O}-*cis*-dioxidomolybdenum(VI)[13] (**1**) was readily made from the H_2bihyat chelator and $MoO_2(acac)_2$, and the final product is air-stable and active toward aerobic sulfide oxidation even after a year of storage in air. In conjunction with experimental results supporting the oxidative mechanism, we also modeled the complete reaction profile wherein there was a close alignment of calculated and measured thermodynamic parameters.

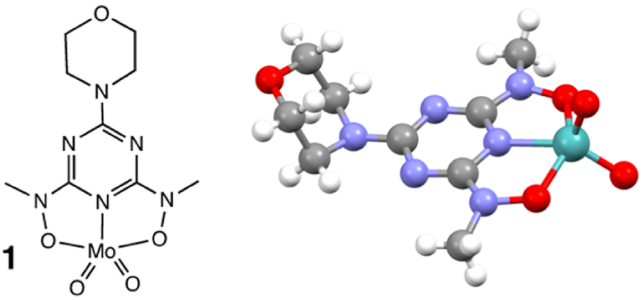

MATERIALS AND METHODS

All NMR spectra were acquired using a Bruker Avance-300 MHz spectrometer at 75.478 and 300.130 MHz for ^{13}C and ^{1}H, respectively. Gas chromatography−mass spectrometry (GC/MS) was acquired on a Varian Saturn 2100T with a Varian 3900 GC; the column was a Factor Four VF-5 ms capillary column (30 m, 0.25 mm). A single-crystal X-ray diffraction structure was collected on a Bruker SMART X2S diffractometer (Supporting Information S1). Cyanuric chloride and *N*-methylhydroxylamine−HCl for ligand (H_2bihyat) synthesis were purchased from TCI, and morpholine and urea hydrogen peroxide were from Sigma-Aldrich. ^{18}O (90 atom %)-labeled aqueous H_2O_2 (3%) was from Icon Isotopes. Triphenylmethanol for trityl hydroperoxide (Ph_3COOH) synthesis was from MCB chemicals, and bis(acetylacetanato)-molybdenum(VI) dioxide was from Strem Chemicals. Aqueous 30% H_2O_2 was from VWR, and MeCN-d_3 was from Cambridge Isotopes. All reagents were used as received, and the synthesis of trityl hydroperoxide[16] followed standard literature protocols. Resonance Raman (RR) spectra were recorded with a McPherson 2061/207 spectrometer equipped with a liquid nitrogen-cooled CCD camera (LN-1100PB, Princeton Instruments) with a 407 nm laser excitation from a Kr laser (Innova I-302, Coherent). A long-pass filter (RazorEdge, Semrock) was used to attenuate the Rayleigh scattering. Room-temperature RR spectra were collected on samples in glass capillaries (1.5−1.8 mm OD, Kimax products) using a 90° geometry. Frequencies were calibrated relative to indene and accurate to ±1 cm^{-1}.

Synthesis of 1. *H_2bihyat Ligand Synthesis.* The synthesis of catalyst **1** used a modified literature protocol.[13] Specifically, 4.6 g of morpholine (53 mmol) was dissolved in 80 mL of tetrahydrofuran (THF). This solution was added dropwise to a chilled mixture of 9.2 g of cyanuric chloride (50 mmol) in 70 mL of EtOAc with vigorous stirring over ice. Afterward, the white suspension was stirred for another 15 min and then gravity-filtered. The filtrate was evaporated in vacuo and recrystallized from isopropanol to yield 3.68 g (16 mmol, 31% yield) of 2,6-dichloro-4-morpholino-1,3,5-triazine; mp: 162−164 °C. This morpholinotriazine (3.68 g, 16 mmol) was dissolved in 50 mL of *p*-dioxane and chilled on ice. A 10 mL aqueous solution of 5.0 g of *N*-methylhydroxylamine−HCl (60 mmol) and 2.7 g of NaOH (54 mmol) was added dropwise to the chilled *p*-dioxane/morpholinotriazine solution and refluxed for 18 h. H_2O (150 mL) was added to yield a white precipitate that was subsequently recrystallized from isopropanol to yield 0.18 g (0.71 mmol, 4.5%) of white H_2biyat ligand; mp: 200−202 °C. ^{1}H NMR ($CDCl_3$): δ 3.37 (6H, CH_3), 3.70−3.81 (m, 8H).

Complex 1 Synthesis. $MoO_2(acac)_2$ (0.25 g, 0.77 mmol) was dissolved in 10 mL of anhydrous THF at room temperature followed by a 10 min N_2(g) sparge. The H_2bihyat ligand (0.20 g, 0.72 mmol) was added to the THF/$MoO_2(acac)_2$ solution, and the orange suspension was stirred under N_2(g) for 5 h. Following gravity filtration, 30 mL of hexane was added to the orange filtrate to yield a bright orange precipitate that was isolated through filtration and washed with hexane. Following recrystallization from MeCN, 0.12 g (0.30 mmol, 39%) of bright orange **1** was recovered.[13] ^{1}H NMR ($CDCl_3$): δ 3.48 (s, 6H, CH_3), 3.76 (t, 4H, −N−C**H**$_2$−CH_2−O), 3.91 (4H, O−**CH**$_2$−CH_2−N). ^{13}C NMR ($CDCl_3$): δ 36.4 (CH_3), 44.8 (N−**C**H_2−CH_2−O), 66.6 (N−**C**H_2−CH_2−O), 159.5, 164.1. Confirmation of the synthesized product was done with diffractometric characterization (Supporting Information S1), in which the crystals were grown from acetonitrile; these crystals were subsequently used for kinetics run.

Kinetics Run. In a typical ^{1}H NMR kinetics run, 0.9 mg of **1** (2.3×10^{-3} mmol) was dissolved in 700 μL of MeCN-d_3 followed by 5 μL of thioanisole **2** (5.9×10^{-2} mmol) or substituted thioanisole; [**1**] = 3.3 mM, [**2**] = 84 mM. The sulfide oxidation was initiated with the addition of an equimolar amount of 30% H_2O_2(aq) (6.7 μL, 2.0 mg, 5.9×10^{-2} mmol) and followed at 30 °C for the Hammett plots. This concentration of **1** meant that only one scan was necessary to yield a suitable ^{1}H NMR with typical delays of 1−2 min. Temperature-dependent studies were done with VT-NMR for the Eyring plots. The samples were equilibrated outside the magnet on a temperature bath for 15 min, then initiated with an equimolar amount of 30% H_2O_2(aq) (6.7 μL, 2.0 mg, 5.9×10^{-2} mmol), and quickly placed in the NMR spectrometer.

^{18}O Labeling Experiments. For the ^{18}O labeling experiments, all manipulations were done in a glovebox with oven-baked glassware. The first labeling experiment employed 100% ^{18}O-labeled **1** for GC/MS analysis of the sulfide (**2**) oxidation product. This commenced with dissolving 5 mg of **1** (1.3×10^{-2} mmol) in 1 mL of dry MeCN-d_3 (ampule sealed from vendor) in the glovebox. This was followed by the addition of 100 μL of ^{18}O water (5.5 mmol) to ensure a large excess of ^{18}O without exceeding the 50% v/v of water to acetonitrile for the aqueous dimerization of **1**, as documented in prior studies.[13] This mixture of **1** in dry MeCN-d_3 with ∼10% (v/v) $^{18}OH_2$ was stirred in the glovebox for 18 h. The next day, a 100 μL portion of the reaction was set aside for resonance Raman analysis, while the rest was subjected to **2** (5 μL, 5.9×10^{-2} mmol) oxidation by Ph_3COOH (15 mg, 5.4×10^{-2} mmol) under anhydrous conditions in the glovebox for 18 h. The sulfide product was subjected to GC/MS analysis. A similar oxidation of **2** was also done with anhydrous urea hydrogen peroxide wherein the sulfoxide product was analyzed by GC/MS.

^{18}O tracking of the trityl hydroperoxide + **1** reaction was done with ^{13}C NMR. In this case, 6 mg (1.6×10^{-2} mmol) of **1** was incubated with a 1:1 mixture of ^{18}O and ^{16}O water (total volume 12 μL) in 600 μL of MeCN to ensure an even mixture of the two oxygen isotopes on the Mo=O functionality. After removal of the solvent in vacuo, 700 μL of MeCN-d_3 was added along with 15 mg (5.4×10^{-2} mmol) of trityl hydroperoxide. This binary mixture was heated at 40 °C for 18 h and then submitted for ^{13}C NMR analysis of the trityl alcohol product.

^{18}O tracking by ^{13}C NMR was repeated with *t*-butyl hydroperoxide as the oxidizing agent in a ternary reaction of **1** + *t*BuOOH + **2**. Here, 5 mg of compound **1** (1.3×10^{-2} mmol) was incubated with a 1:1 mixture of ^{18}O and ^{16}O water (total volume 100 μL) in 1 mL of MeCN-d_3 overnight at room temperature in the glovebox. This ^{18}O-labeled **1** was then incubated with 7 μL of 70% *t*BuOOH (5.4×10^{-2} mmol) and 5 μL of **2** (5.9×10^{-2} mmol) at 40 °C for 18 h.

The second ^{18}O labeling experiment used ^{18}O-labeled aqueous H_2O_2 (3%) that was 90% isotopically (^{18}O) enriched. Catalyst **1** (1 mg, 2.4×10^{-3} mmol) was dissolved in 800 μL of MeCN-d_3 along with 2.5 μL of thioanisole **2** (3.0×10^{-2} mmol). This was followed by 25 μL of ^{18}O-labeled H_2O_2, and the reaction was run for 18 h at 30

https://doi.org/10.1021/acs.inorgchem.1c00145
Inorg. Chem. 2021, 60, 7762−7772

°C; ^{1}H NMR was used to track the progress of the reaction to ensure production of the sulfoxide. As a control, a parallel was run using unlabeled 30% H_2O_2(aq) that was diluted 10-fold with D_2O.

Computational Modeling. DFT calculations were performed in Gaussian 16.[17] Structures were built using GaussView,[18] and computed structures were rendered using CYLView.[19] All calculations used the B3LYP-D3 functional with the def2-SVP basis set and SMD solvent model for acetonitrile.[20,21] This model includes Grimme's D3 (original damping) dispersion correction.[22] Catalyst **1** was assembled from crystallographic coordinates, and transition states were located using either coordinate scans or the QST3 algorithm.[23] Conformational searches were conducted manually to locate the lowest-energy conformation of each structure. IRC calculations were performed to verify that transition states connected to the correct intermediates.

Thermal corrections to enthalpy and Gibbs free energy were calculated from unscaled vibrational frequencies at room temperature (298 K). A default pressure of 1 atm was used in Gaussian, and an empirical correction was applied to correct for the overestimation of translational entropy in solution.[24] This correction was made by adding 18 kJ/mol (4.3 kcal/mol) to the free energy of all structures, which has the effect of decreasing the entropic cost of bimolecular steps by this amount. This treatment, first proposed by Martin et al.,[25] is derived from $RT\ln(c_{soln}/c_{gas})$, where c_{gas} is the standard molar concentration in the gas phase (1 atm or 0.041 mol/L) and c_{soln} is the molar concentration of pure water at room temperature (55.6 mol/L). This approach has been successfully applied to density functional theory (DFT) studies of catalytic reactions and shown to give ΔS values for bimolecular reactions that more closely align with experiment.[26]

For comparison to experimental resonance Raman spectra, vibrational frequencies were scaled by a factor of 0.97. This value is intermediate in recommended values for B3LYP with double-zeta basis sets (typically 0.96−0.98).[27,28] Moreover, this scaling factor provides a good agreement between the computed and experimental values of ν(Mo═O) in catalyst **1**.

RESULTS AND DISCUSSION

The two fundamental questions are the mode of oxygen transfer to the sulfide and the thermodynamics of sulfide oxidation. These questions are taken within the context of an oxidation reaction on a model sulfide thioanisole (**2**) oxidation (R_1 = C_6H_5, R_2 = CH_3) (eq 1). This proof-of-concept oxidation on sulfide **2** suggests a route that goes through a η^1-peroxo pathway. The results are presented in five sections that look at (a) peroxide activation of catalyst **1**, (b) the outcome of using ^{18}O-labeled **1** in eq 1, (c) sulfide oxidation promoted by ^{18}O-labeled-H_2O_2, (d) key thermodynamic parameters, and finally (e) computational results that support the hypothesized oxygen transfer reaction. While the sections (a) and (b) downplay a hypothesized η^2-peroxo pathway, the results set in the section (c) provide ^{18}O labeling results consistent with a η^1-peroxo species that is key in the oxygen transfer reaction.

Activation of 1 by Peroxides. Complex **1** by itself is inactive for sulfide oxidation and requires activation by a peroxide in a transformation reminiscent of prior oxazine systems of $MoO(OO)_2$ complexes.[29] The title catalyst **1**[13] is a five-coordinate Mo dioxido complex with the central metal in a pseudo-trigonal bipyramid geometry. This is in contrast to other dioxomolybdenum(VI) complexes that have a six-coordinate octahedral metal geometry.[30] In terms of the dioxido ligation, the oxygen atoms undergo facile exchange with water,[31] as shown in the resonance Raman spectrum of **1** (Figure 1) when incubated with ^{18}O-labeled water[32] in acetonitrile. Prior studies on both η^2- and η^1-peroxo Mo(VI) complexes indicate a Mo═O stretch in the 940−960 cm^{-1} range.[11] The ν(Mo═O) mode in **1** is identified at 941 cm^{-1} as

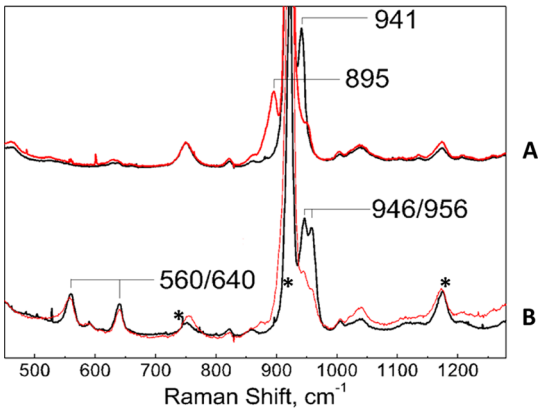

Figure 1. Room-temperature resonance Raman spectra of **1** in acetonitrile (CH_3CN) with 10% $^{16}OH_2$ (A, top black trace) or $^{18}OH_2$ (A, top red trace) obtained with a 407 nm laser excitation. Addition of H_2O_2(aq) results in the appearance of two new bands at 560 and 640 cm^{-1} (B, in acetonitrile with 10% $^{16}OH_2$ (black trace) or $^{18}OH_2$ (red trace)). The asterisk (*) labels the intense Raman band of acetonitrile at 910 cm^{-1} as well as other solvent bands.

this band downshifts to 895 cm^{-1} after a short (<1 min) incubation of **1** in a 10:1 mixture of acetonitrile and $^{18}OH_2$. This 46 cm^{-1} downshift (95.1%) exactly matches the calculated shift (Supporting Information S1) from Hooke's law for a diatomic harmonic oscillator (Figure 1A). Oxygen lability in Mo═O moieties has been reported previously for a molybdenum dioxido complex[33] and serves as a key tool for oxygen tracking in sulfide oxidation. In addition, Figure 1B also shows that upon addition of H_2O_2(aq) two new bands appear at 560 and 640 cm^{-1}. While these frequencies have been attributed to the η^2-peroxo functionality (i.e., Mo−O vibration),[11] both η^1- and η^2-peroxo functionalities have been implicated in epoxidation[34] and sulfide oxidations. This report addresses both types of peroxo groups with regard to their validity in sulfide oxidation by catalyst **1**. In connection with Figure 1B, the added bands from the Mo−O vibration (i.e., new bands at 560 and 640 cm^{-1}) may contribute to the main Mo═O vibration (941 cm^{-1}) as delineated later (the ^{18}O-Labeled H_2O_2(aq) section) with ^{18}O-labeled H_2O_2 addition. Note that the disappearance of the Mo═^{18}O 895 cm^{-1} band (Figure 1B) upon the addition of H_2O_2 (aq) is due to the excess ^{16}O water exchanging (washing) out the ^{18}O-labeled **1**.

Thioanisole (**2**) serves as a model sulfide to probe the sulfur oxidation by **1** in the presence of peroxide (eq 2)

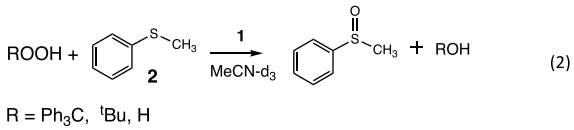

(2)

R = Ph_3C, ^{t}Bu, H

The most active peroxide was aqueous H_2O_2 (27−30%) followed by urea hydrogen peroxide(s),[35] aqueous *t*-butyl hydroperoxide (70%), and finally trityl hydroperoxide(s)[16] −Ph_3COOH. Oxidation of **2** by **1** with either *t*BuOOH(aq) or trityl hydroperoxide yielded the corresponding alcohols *t*BuOH or trityl alcohol, respectively. Since H_2O_2(aq) was the most convenient oxidizing reagent, future sulfide oxidation reactions were done by an equimolar (relative to **2**) amount of H_2O_2(aq). Neither compound **1** nor H_2O_2(aq) alone oxidizes **2**; the two in conjunction oxidize sulfide **2**, and the oxidations are initiated with the addition of H_2O_2(aq). Oxidation of **2** in CD_3CN was followed by ^{1}H NMR (Figure 2), and the

https://doi.org/10.1021/acs.inorgchem.1c00145
Inorg. Chem. 2021, 60, 7762−7772

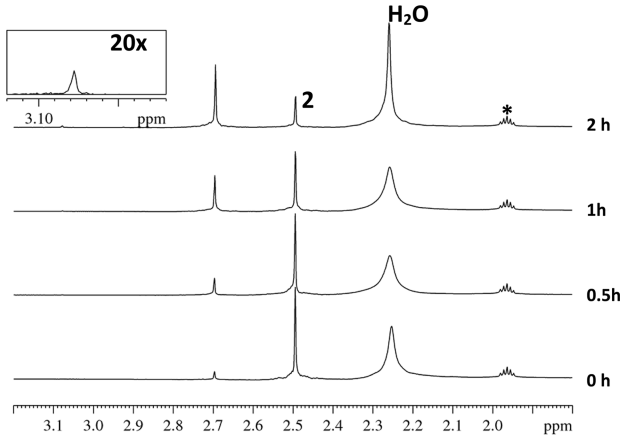

Figure 2. Aerobic oxidation (30 °C) of thioanisole (**2**) to methyl phenyl sulfoxide (eq 2) by **1** in acetonitrile-d_3 (*) to form the sulfoxide at 2.7 ppm. The conditions are described in materials, and singlets represent methyl groups. The inset at a 2 h mark shows the corresponding sulfone (3.08 ppm).

decrease of **2** was fitted to a first-order decay for two and a half to three half-lives (2.5−3 $\tau_{1/2}$) with a 4% catalyst loading (**2** to **1** ratio of ∼25:1). These kinetics results were essential for understanding the fundamental thermochemistry of eq 2 set out in the section (d). The minute amount of the sulfone formation (Figure 2) is less than 0.5% of the starting **2** and represents negligible overoxidation.

One of the key concerns is the possibility of the loss of the ligand from **1**.[13] As such, the downfield region of the ligand for **1** was tracked during the oxidation of **2**.

The ^{1}H signals in the 3.4−4.0 ppm range for **1** (Figure 3) do not exhibit the ^{1}H NMR signal displacements attributed to ligand loss from **1**. Specifically, the methyl singlet of the free H_2bihyat ligand (3.40 ppm) is not evident upon the oxidation of **2**, as seen in the previously reported work of **1** hydrolysis.[13] Moreover, the previous aqueous hydrolysis investigation[13] was conducted in the CD_3CN solution with >50% (v/v) D_2O; all our oxidation reactions with H_2O_2(aq) used less than 1% (v/v) of aqueous H_2O_2. The broadening of the ^{1}H signals of the catalyst (3.65−3.9 ppm) may be due to the formation of an active peroxo intermediate.

^{18}O-Labeled Catalyst 1. In connection with possible mechanistic pathways, we took advantage of the oxygen exchangeability of Mo═O and installed ^{18}O on **1** to track the fate of these oxo atoms. Our results do not support an active η^2-peroxo active species set in Scheme 1, and various attempts were taken to promote the formation of this hypothetical complex. Scheme 1 sets out two possible pathways for making the putative active η^2-peroxo active species. They both start with **1** reacting with hydrogen peroxide to form **3** through a proton transfer to the terminal [Mo═O ↔ $M^+\cdots O^-$] oxo functionality. Compound **3** can form a Mo(VI) η^2-peroxo species through two possible routes. In route A, the hydroxyl of **3** acts as a base/nucleophile and abstracts the Mo−OOH proton of **3** to form the Mo(VI) η^2-peroxo complex **4a**. The alternate route (B) uses the weak O−O peroxo bond of **3** to form η^2-species **4**. Such a pathway would install the ^{18}O label on a η^2-peroxo functionality of **4b**. A detailed description of complex **4** (a and b) is provided later in the computational discussion (the Computational Modeling of Sulfide Oxidation by **1** and H_2O_2 via Intermediate **3** section).

In connection with route A (Scheme 1), Mimoun[33] supported the formation of a Mo(η^2-OO) complex similar to that of **4a** when ^{18}O-labeled MoO_2Cl_2(Pic)$(HMPT)_2$ (HMPT = hexamethylphosphorus triamide; Pic = pyridine-2-carboxylate) was treated with Ph_3COOH. The trityl group served to stabilize a possible carbocation intermediate for the hydroxyl transfer, and their results revealed ^{18}O incorporation in the product trityl alcohol (Ph_3COH) (eq 3)

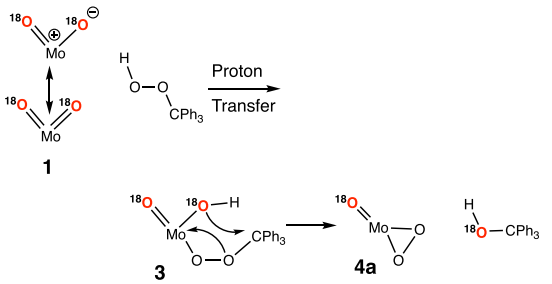

(3)

To this end, an overnight incubation of **1** in a 1:1 mixture of ^{16}O and ^{18}O water (total volume 12 μL) was followed by treatment with trityl hydroperoxide. The mixture of labeled and unlabeled water ensured an equal probability of ^{16}O and ^{18}O labeling of the trityl (Ph_3COH) alcohol product. This reaction (eq 3) should manifest itself with the α-carbon signal bearing a 1:1 mixture of C−^{18}O and C−^{16}O in which the ^{13}C

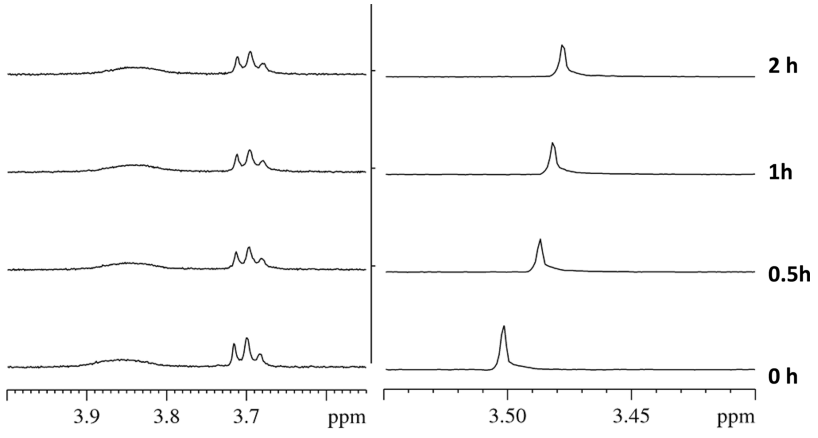

Figure 3. ^{1}H NMR (3.4−4.0 ppm range) of ligand portion of **1** while oxidizing **2** under the conditions described in Figure 2. The expanded 3.40−3.55 ppm region indicates no evidence of the free H_2bihyat ligand.

https://doi.org/10.1021/acs.inorgchem.1c00145
Inorg. Chem. 2021, 60, 7762−7772

Scheme 1. Possible Routes for Side-on Peroxo Formation

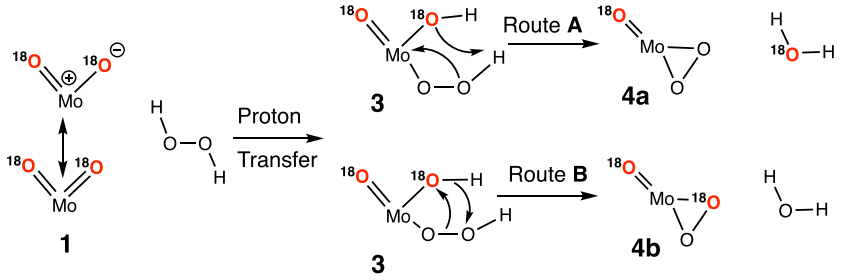

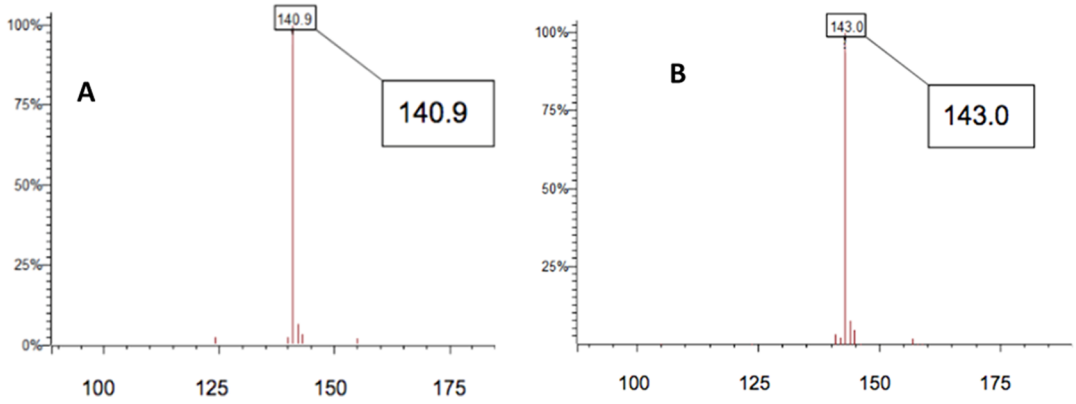

Figure 4. GC/MS of the product methyl sulfoxide (MW = 141) when unlabeled **1** is treated with **2** with either unlabeled or ^{18}O-labeled 3% H_2O_2(aq) in MeCN-d_3. Spectrum (A) controls oxidation when unlabeled 3% H_2O_2(aq) was used. Spectrum (B) controls the identical oxidation with ^{18}O-labeled H_2O_2(aq).

NMR spectrum has two signals (82 ppm) separated by 0.05 ppm.[36] A similar oxygen-tracking strategy was employed in probing the mechanism of parathion hydrolysis by a molybdenum(IV) metallocene.[37] The ^{13}C NMR shows the formation of the trityl alcohol with the formation of the 82 ppm signal of the methine α-carbon. However, this 82 ppm signal revealed no isotopic ^{18}O/^{16}O mixture due to BOTH C−^{18}O and C−^{16}O bondings; it was a clear singlet indicative of no mixed ^{18}O/^{16}O attachment (Supporting Information S3).

An alternate mode for trityl alcohol formation is proposed in Scheme 1 (route B) in which the ^{18}O label is installed on the η^2-peroxo functionality of **4b** and not on the product alcohol. Intermediate **4b** would be the active species that oxidizes the sulfide by the ^{18}O-labeled peroxo functionality. This scheme would then install the ^{18}O oxygen on the sulfoxide product. Therefore, incubation of an acetonitrile solution-d_3 of **1** in ^{18}O water (10% by volume) under rigorously anhydrous conditions (i.e., glovebox and oven-backed glassware to avoid ^{16}O water contamination) showed that all of the Mo=O stretches were indeed Mo=^{18}O, as demonstrated by resonance Raman (i.e., no Mo=^{16}O stretches were seen at 941 cm^{-1}; Supporting Information S4). This (100%) ^{18}O-labeled **1** was incubated overnight with **2** in the presence of dry Ph_3COOH under anhydrous conditions and then submitted to GC/MS to examine the sulfoxide oxidation product. The mass spectrum (Supporting Information S5) revealed no ^{18}O incorporation in the sulfoxide. This negative result is inconsistent with the route B of Scheme 1 and further diminishes a possible η^2-peroxo intermediate.

As a control, the resonance Raman spectrum of the reaction of ^{18}O-labeled **1** with Ph_3COOH showed that ^{18}O incorporation in the Mo=O remains intact (Supporting Information S4), as evidenced by the Mo=^{18}O 895 cm^{-1} stretch; the ^{18}O of **1** did not exchange out into the product alcohol or the sulfoxide product. In addition, a ternary 18 h reaction with a 50:50 ^{18}O/^{16}O-labeled **1** (5 mg, 1.2 × 10^{-2} mmol) + **2** (5 μL, 5.9 × 10^{-2} mmol) + Ph_3COOH (14 mg, 5.0 × 10^{-2} mmol) showed no ^{18}O incorporation into the Ph_3COH product alcohol, as evidenced with ^{13}C NMR; the methine signal at 82 ppm was just a singlet. The absence of ^{18}O incorporation was also seen in the ternary reaction of ^{18}O/^{16}O-labeled **1** (5 mg, 1.2 × 10^{-2} mmol) + **2** (5 μL, 5.9 × 10^{-2} mmol) + *t*BuOOH (5.4 × 10^{-2} mmol); the *t*BuOH products appear as just a singlet at 68.6 ppm (Supporting information S6).

^{18}O-Labeled H_2O_2(aq). While the aforementioned ^{18}O labeling results (i.e., ^{18}O-labeled **1**) do not suggest an active η^2-peroxo active species, we present results consistent with the notion that the initial η^1-hydroperoxo intermediate **3** (R = H in eq 3) is the active species in sulfide oxidation

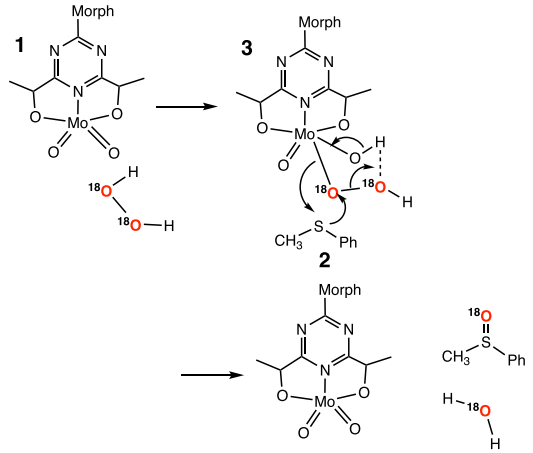

(4)

https://doi.org/10.1021/acs.inorgchem.1c00145
Inorg. Chem. 2021, 60, 7762−7772

The pathway hypothesized in eq 4 suggests ^{18}O incorporation into **2** when catalyst **1** is unlabeled and the H_2O_2 is ^{18}O-labeled. As such, ^{18}O−3% H_2O_2(aq) was employed that was 90% atom (^{18}O)-labeled. First, control experiments with 3% H_2O_2 alone showed no thioanisole oxidation in the absence of catalyst **1**. In addition, ^{18}O-labeled 3% H_2O_2(aq) alone shows no oxygen exchange with the methyl phenyl sulfoxide product, as evidenced by GC/MS. A parallel control reaction was run, in which catalyst **1** (no ^{18}O label) was dissolved in MeCN-d_3 with **2** along with an equimolar amount of (no ^{18}O label) H_2O_2(aq). After an 18 h reaction at 30 °C, ^1H NMR of the reaction showed it to be 50% complete. GC/MS analyses in Figure 4 show both the control reaction (i.e., Figure 4A with no ^{18}O label) and the key reaction with ^{18}O-labeled H_2O_2(aq) (Figure 4B). The mass spectrum clearly shows ^{18}O incorporation in the methyl phenyl sulfoxide product.

In the proposed sulfide oxidation, the hydroperoxide (HOOH) transfers the proton to one of the terminal molybdenum dioxo functionalities of **1** to form **3** (eq 3); the HOO^- group binds as the sixth ligand in a η^1-fashion. In this regard, the reaction of **1** with ^{18}O-labeled H_2O_2 in MeCN-d_3 was probed with resonance Raman spectroscopy. As observed earlier in Figure 1, when **1** is treated with H_2O_2, new Raman bands appear at 556 and 638 cm^{-1} and the ν(Mo═O) shifts from 940 to 958 cm^{-1} (Figure 5B, blue trace). In contrast,

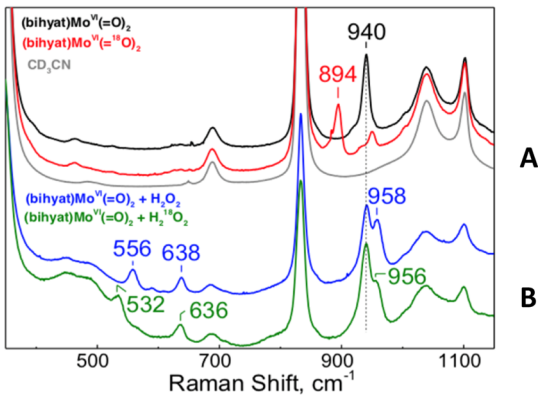

Figure 5. Resonance Raman of compound **1** in MeCN-d_3 treated with either (A) ^{18}O-labeled H_2O or (B) 3% H_2O_2(aq)-hydrogen peroxide. (A) Compound **1** in black, **1** + $^{18}OH_2$ in red, and MeCN-d_3 in gray. (B) Compound **1** treated with H_2O_2(aq) (blue trace) or with ^{18}O-labeled H_2O_2(aq) (green trace).

when **1** is exposed to $H_2{}^{18}O_2$, the new resonance Raman bands appear at 532 and 636 cm^{-1} and the ν(Mo═O) shifts to 956 cm^{-1} (Figure 5B, green trace). The 24 cm^{-1} downshift of the 556 cm^{-1} band with ^{18}O-labeled H_2O_2 identifies this mode as possibly ν(Mo−O_2). The calculated Mo−$^{18}O_2$ stretch (95.1% of Mo−$^{16}O_2$ from Supporting Information S1) would be at 529 cm^{-1} that compares favorably with the observed 532 cm^{-1}. The much smaller 3 and 2 cm^{-1} downshifts of the 638 and 940 cm^{-1} bands, respectively, suggest weak contributions of the peroxide ligand to these modes that otherwise are dominated by the (bihyat)Mo═O vibrations.

When the aforementioned result is coupled with the mass spectral results (Figure 4) of the methyl phenyl sulfoxide (^{18}O present) product, it suggests that **3** oxygenates the sulfide with the hydrogen peroxide oxygen. The proposed mechanism (eq 4) has the Mo(VI) in complex **3**, which serves as a Lewis acid to enhance the oxidizing ability of this η^1-peroxo group. In the next step, the sulfide approaches the coordinated α-oxygen of **3** followed by sulfur nucleophilic attack on this electrophilic oxygen to regenerate **1** with the concomitant formation of the sulfoxide and water. In terms of the steric hindrance of intermediate **3** toward sulfide oxidation, the proposed sulfide oxidation in eq 4 is also consistent with the relative reaction rates by the peroxides where H_2O_2 > *t*BuOOH ≫ Ph_3COOH.

Previous investigations on olefin epoxidation by ^{18}O-labeled vanadium and molybdenum oxo catalysts interpreted the absence of ^{18}O in the products as indicative of an active alkyl peroxide species (i.e., M(η^1-OOR)).[34,35] It should be noted that dry UHP + ^{18}O-labeled **1** displayed no ^{18}O incorporation in the sulfoxide product as well. A similar oxidation of **2** by H_2O_2(aq) (Supporting Information S5) is problematic because of the rapid Mo═O oxygen exchange (<1 min) with the excess ^{16}O water in aqueous H_2O_2, as shown in Figure 1B. The proposed oxidative reaction proposed in eq 4 could be general for other peroxidations. For example, sulfide oxidation by sugar-based *cis*-dioxo Mo(VI) complex[38] has been reported and speculated to proceed through a η^2-peroxo intermediate. Alternatively, both Kühn and Sharpless have invoked a η^1-alkylperoxo complex as the key intermediate in olefin epoxidation reactions with *t*BuOOH.[34,40] Furthermore, Bagherzadeh[39] and Kühn[40] proposed an oxidative process identical to eq 4 for olefin epoxidation by *cis*-dioxomolybdenum(VI)-oxazoline and $MoO_2Cl_2(DAB)_2$ (DAB; DAB = 1,3-diazabutadiene) complexes, respectively. A similar mechanism to eq 4 was also proposed for the sulfide oxidation by $CpMoO_2Cl$ in the presence of CH_3COOH.[41] As a strictly computational work, there was no experimental evidence to support the fate/source of the oxygen. In this submission, we show unequivocal oxygen (^{18}O) incorporation in the sulfide → sulfoxide oxidation as spelled out in eq 4, and this is complemented and supported with computational results.

Kinetics of Sulfide Oxidation by 1. The hypothesized mechanism in eq 4 treats the sulfide as a nucleophile, which is supported by the kinetics measurements that further provide thermochemical parameters to support computational modeling. The rates of sulfide oxidation were sufficiently slow enough that initial rates were easily measured. As such, a Hammett linear free-energy relationship[42] was measured for thioanisole derivatives containing electron-donating and electron-withdrawing groups in the para position (Figure 6).

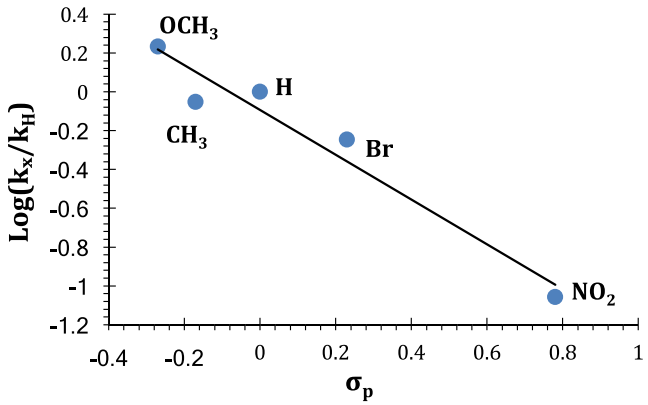

Figure 6. Linear free-energy Hammett plot for the oxidation of para-substituted thioanisoles by **1**. Raw kinetics data are in Supporting Information S7. The reactivity constant, ρ, (slope), is −1.2 ± 0.2.

https://doi.org/10.1021/acs.inorgchem.1c00145
Inorg. Chem. 2021, 60, 7762−7772

To a first approximation, there is a linear relationship in the rate of sulfide oxidation with the Hammett constant of the para-substituent. In addition, the negative slope means the transition state favors electron-donating groups. This is consistent with the hypothesis that sulfur acts as a nucleophile in attacking the electropositive molybdenum-peroxo functionality, as seen in prior work.[8] In terms of comparisons with similar sulfide oxidations (i.e., **2** + catalyst + H_2O_2) by other metal peroxo complexes, a Hammett reactivity constant (ρ) of -1.2 ± 0.2 in Figure 6 falls very close to the corresponding diperoxo-molybdate dimer $[\{MoO(O_2)_2\}_2(\mu\text{-}O)]^{2-}$ that has a ρ of -1.06.[8] The tungstate diperoxo complex[43] $SeO_4\{WO(O_2)_2\}_2^{2-}$ yielded a ρ of -0.62 for the similar sulfide oxidation. All three of these group 6 metal complexes yield a Hammett linear free-energy plot indicative of a sulfide nucleophile attacking an electrophilic peroxidic oxygen ligand of the metal catalyst. Prior work by Di Furia[44] on **2** showed the same relationship with para-substituted thioanisole that yielded a negative ρ.

The exponential decay rates (Supporting Information S8) in eq 2 with 4% of **1** loading provided first-order rate constants for determining key thermodynamic activation parameters consistent with the proposed oxidation mechanism. Comparisons with other metal complexes show similarities and differences with regard to these activation parameters. In terms of a η^2-Mo(OO) peroxo complex,[45] prior investigations of **2** were carried out with oxodiperoxo (pyridine-2-carboxylato)-molybdate(VI) bis(pyridine-2-carboxylic acid) monohydrate (**5**, Figure 7), and an Eyring plot yielded an E_a of 56.5 ±1.6 kJ/mol in dichloroethane. The standard deviations were calculated based on the rate constants (30–60 °C) reported by Di Furia.[44] In our oxidation of **2** by **1**, an E_a of 63.0 ± 5.2 kJ/mol (Figure 7) was obtained, which is higher (i.e., >1 standard deviation) than the activation energy obtained with complex **5**.

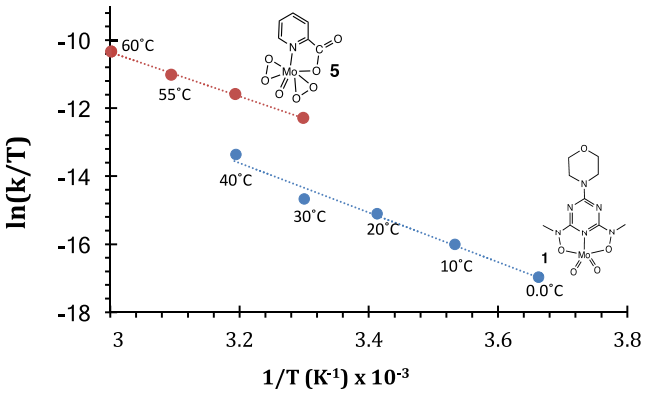

Figure 7. Eyring plots for the oxidation of **2** by the oxodiperoxo (**5**) and dioxo (**1**) molybdenum(VI) complexes. Data for **2** oxidation by **5** were taken from ref 44b and have a slope of -6.5×103. The slope for **1** oxidation was -7.23 (± 0.62) $\times 10^3$; uncertainty values were taken from LINEST, and raw data are in Supporting Information S8.

It is worth noting that differences in the E_a values between **2** and **5** arise from Mo(VI) systems that are distinctively different with regard to the Mo(OO) peroxo functionality. The Eyring plot gives an entropy of activation suggestive of an associative rate-determining step. We calculate a $\Delta S^{\ddagger}$ of -124 J/mol·K from prior kinetics data (Table 1 in ref 44b) in the oxidation of **2** by **5**; Di Furia and co-workers attribute the negative $\Delta S^{\ddagger}$ to a bimolecular rate-determining step.[44] As such, we calculate a $\Delta S^{\ddagger}$ of -117 ±1.7 J/mol·K for **2** oxidation by **1**, which falls reasonably close to the aforementioned $\Delta S^{\ddagger}$ (i.e., **2** oxidation by **5**), especially given the different ligation about the Mo(VI) center for **1** versus **5**. These thermochemical results compare very favorably with the computational modeling of eq 4 and are summarized in the Computational Modeling of Sulfide Oxidation by **1** and H_2O_2 via Intermediate **3** section.

Computational Modeling of Sulfide Oxidation by 1 and H^2O^2 via Intermediate 3. DFT calculations were employed to confirm and further elucidate the proposed sulfide oxidation mechanism in eq 4. Catalyst **1** was optimized at the B3LYP-D3/def2-SVP level using the SMD model for acetonitrile, and the calculated Mo=O vibrational frequency[45] of 938 cm^{-1} closely matches experiment (Table 1). As shown in Figure 5, the addition of H_2O_2 leads to new bands at 958, 638, and 556 cm^{-1}, proposed to correspond to Mo=O and M–O bands in η^1-hydroperoxo complex **3**. DFT calculations indicate that **3** exists in several low-energy conformations (within about 2 kJ/mol). The lowest free-energy conformation is shown in Table 1 with computed vibrational frequencies, and additional conformations are shown in the Supporting Information. The Mo=O band shifts to 957 cm^{-1}, in excellent agreement with experiment. Calculations show that the band at 634 cm^{-1} (638 cm^{-1} in Figure 5 and 640 cm^{-1} in Figure 1B) corresponds to a Mo–O(bihyat) stretch in some cases coupled with Mo–OH, which is consistent with the fact that this band does not shift significantly when ^{18}O-labeled H_2O_2 is used (Figure 5). The Mo–OOH stretch is calculated to be at about 498 cm^{-1}, which is not clearly visible in the RR spectrum. It is worth noting that these molecules contain many other vibrational frequencies, but our focus is on explaining the observed bands, rather than simulating the full resonance Raman spectrum.

The alternative η^2-peroxo complex **4** was also calculated and shares some of the same bands. However, the Mo=O stretch is calculated to be at a significantly higher frequency (984 cm^{-1}), which is not consistent with the experimental spectrum, lending further support to the η^1-mechanism in eq 4.

Next, sulfide oxidation via η^1-hydroperoxo complex **3** was modeled to obtain theoretical activation parameters (Figure 8). Outer-sphere coordination of H_2O_2 with the catalyst to give **1-H_2O_2** is slightly exergonic. Proton transfer and coordination of the hydroperoxo ligand give complex **3** via $\mathbf{TS}_{1-3}$. This and the subsequent transition state are stabilized by internal hydrogen bonds between a hydroxyl group and an oxygen in the bihyat ligand. The rate-determining step of the oxidation is nucleophilic attack of the sulfide on the hydroperoxo ligand via $\mathbf{TS}_{3-6}$, forming the sulfoxide product and displacing a hydroxyl group to the apical position in complex **6**. A proton transfer via $\mathbf{TS}_{6-1}$ liberates H_2O and sulfoxide product and regenerates catalyst **1**.

In a minor revision to the mechanism in eq 4, DFT calculations show that the attack of the sulfide and this final proton transfer are actually two distinct steps. This two-step mechanism (sulfide attack followed by proton transfer to regenerate **1**) is also distinct from a previous computational study of sulfide oxidation by $CpMoO_2Cl$,[41] which closely follows eq 4. In the current case, a 14-electron complex **3** features a vacant coordination site for the departing hydroxyl group in $\mathbf{TS}_{3-6}$, which is not possible for the analogous 16-electron complex derived from $CpMoO_2Cl$. Migration of the hydroxyl group to the Mo center likely leads to a more facile

https://doi.org/10.1021/acs.inorgchem.1c00145
Inorg. Chem. 2021, 60, 7762–7772

Table 1. Comparison of Experimental and Calculated Vibrational Frequencies (in cm^{-1})

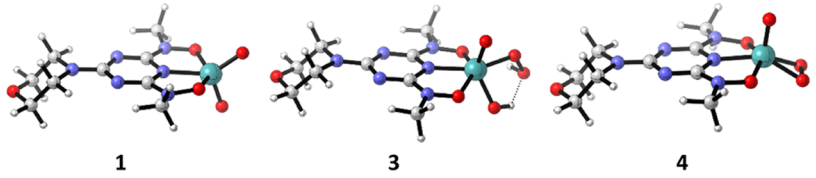

	1	3	4
Experimental frequencies	941	958, 638, 556	
DFT frequencies			
Mo═O	938	957	984
Mo−O(bihyat)	616	634, 617	631, 645
Mo−OH		563	
Mo−OO		498	570

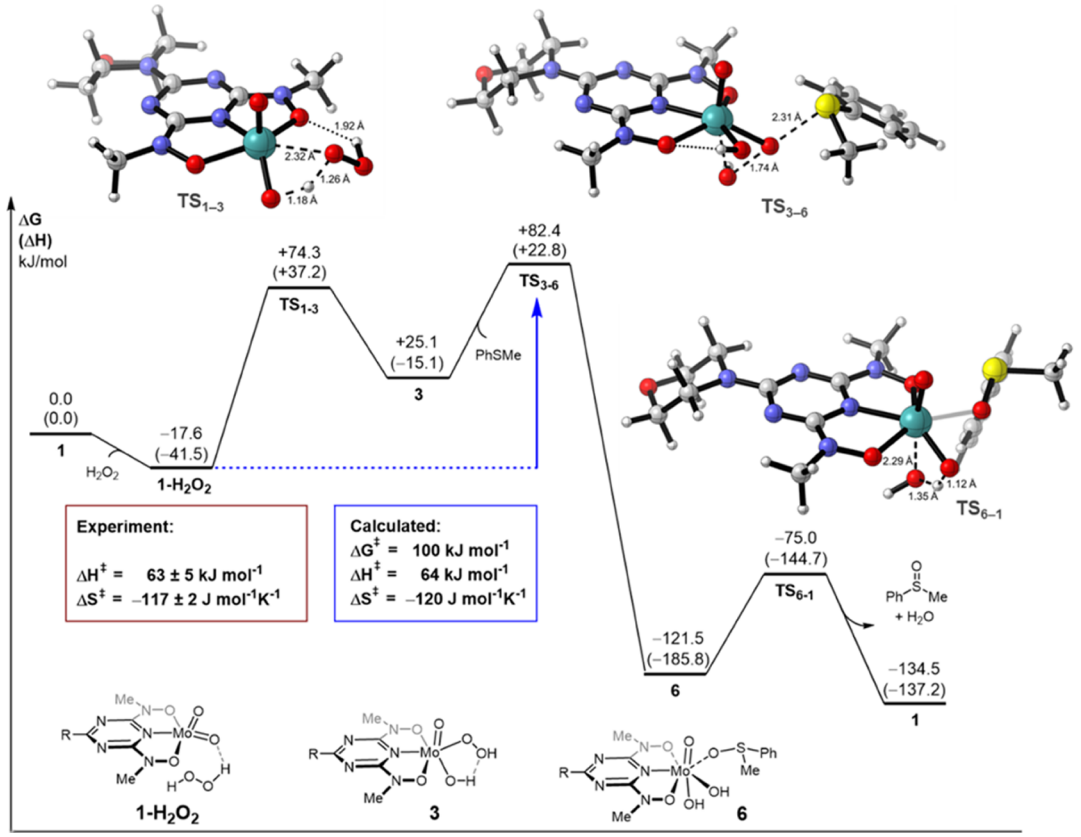

Figure 8. Calculated energy profile for sulfide oxidation via hydroperoxo complex **3**. Gibbs free energies and enthalpies (in parentheses) in kJ/mol, calculated with B3LYP-D3/def2-SVP with SMD (acetonitrile). Experimental activation energies in the red box are derived from the Eyring plot (Figure 7).

oxidation, as the barrier for $\mathbf{TS_{3-6}}$ is significantly lower than the sulfide oxidation barrier previously computed for $CpMoO_2Cl$.

According to the DFT calculations, the rate-limiting step is the nucleophilic attack of sulfide on hydroperoxo complex **3**, in accord with the Hammett study in Figure 6. Because coordination of H_2O_2 is exergonic, the free-energy barrier controlling turnover is 100 kJ/mol ($\mathbf{1\text{-}H_2O_2}$ to $\mathbf{TS_{3-6}}$). The components of this calculated barrier ($\Delta H^{‡}$ = 64 J/mol and $\Delta S^{‡}$ = −120 J/mol·K) are remarkably close to the experimentally determined E_a (63.0 ± 5.2 kJ/mol) and $\Delta S^{‡}$ (−117 ±1.7 J/mol·K) from the Eyring plot in Figure 7. This exceptional match between experiment and theory strongly supports the proposed mechanism in eq 4.

The alternative mechanism proceeding through η^2-peroxo complex **4** (Scheme 1) was also modeled. However, the free-energy barrier is somewhat higher and the computed activation parameters ($\Delta H^{‡}$ = 92 kJ/mol, $\Delta S^{‡}$ = −36 J/mol·K) do not match experiment (see Supporting Information S9), providing further evidence against this mechanism.

CONCLUSIONS

A new application for the pincer-like, triazine Mo(VI) dioxo complex is reported, where it readily oxidizes sulfides to the sulfoxide under mild catalytic conditions. This air-stable Mo(VI) coordination complex is activated with a variety of peroxides. Oxygen-18 labeling experiments do not point to a η^2-peroxo intermediate. Instead, ^{18}O-labeled H_2O_2 results are consistent with an activated η^1-hydroperoxo Mo(VI) complex

https://doi.org/10.1021/acs.inorgchem.1c00145
Inorg. Chem. 2021, 60, 7762−7772

initially formed in a proton transfer to the Mo=O moiety. This yields an activated and electropositive α-oxygen that is attacked by the sulfur nucleophile. Further support for this model of sulfide oxidation comes from DFT calculations that yield thermochemical activation parameters very close to the measured $\Delta S^{\ddagger}$ and $\Delta H^{\ddagger}$ values. Current efforts are devoted toward the improvement of this chemistry with other group 6 systems similar to complex **5**.

■ ASSOCIATED CONTENT

Supporting Information

The Supporting Information is available free of charge at https://pubs.acs.org/doi/10.1021/acs.inorgchem.1c00145.

Detailed crystallographic data; Raman spectra; calculations for determining Mo=O stretch with ^{18}O labeling; ^{13}C NMR spectra; mass spectra; kinetics data for Hammett and Eyring plots; and computational details and energies of computed structures (PDF)

Coordinates of all computed structures (XYZ)

■ AUTHOR INFORMATION

Corresponding Author

Louis Y. Kuo − *Department of Chemistry, Lewis & Clark College, Portland, Oregon 97219, United States;* orcid.org/0000-0002-3695-8339; Email: kuo@lclark.edu

Authors

Cayden X. Bullock − *Department of Chemistry, Lewis & Clark College, Portland, Oregon 97219, United States*

Cooper S. Jamieson − *Department of Chemistry, Lewis & Clark College, Portland, Oregon 97219, United States*

Pierre Moënne-Loccoz − *Department of Chemical Physiology and Biochemistry, Oregon Health Science University, Portland, Oregon 97239, United States*

Buck Taylor − *Department of Chemistry, University of Portland, Portland, Oregon 97203, United States;* orcid.org/0000-0002-6586-3865

Jordan A. M. Gonzalez − *Department of Chemistry, Lewis & Clark College, Portland, Oregon 97219, United States*

Ellie A. Draves − *Department of Chemistry, Lewis & Clark College, Portland, Oregon 97219, United States*

Complete contact information is available at: https://pubs.acs.org/10.1021/acs.inorgchem.1c00145

Notes

The authors declare no competing financial interest.

■ ACKNOWLEDGMENTS

This work was funded by ACS-PRF award 58343-UR3, and the author acknowledges Professor Edward Valente (U. of Portland) for the final crystallographic characterization of **1** and Tim Smale (L&C) for computer support. Computations were performed on SDSC Comet with resources provided by the Extreme Science and Engineering Discovery Environment (XSEDE), which is supported by NSF award ACI-1548562. The authors also thank the reviewers for insightful manuscript recommendations.

■ REFERENCES

(1) Zhong, Q.; Shen, H.; Yun, X.; Chen, Y.; Ren, Y.; Xu, H.; Shen, G.; Ma, J.; Tao, S. Effects of International Fuel Trade on Global Sulfur Dioxide Emissions. *Environ. Sci. Technol. Lett.* **2019**, *6*, 727−731.

(2) Dignon, J. NO_x and SO_x emissions from fossil fuels: A global distribution. *Atmos. Environ., Part A* **1992**, *26*, 1157−1163.

(3) Ahmed, I.; Jhung, S. H. Adsorptive desulfurization and dinitrogenation using metal−organic frameworks. *J. Hazard. Mater.* **2016**, *301*, 259−276.

(4) (a) Eßer, J.; Wasserscheid, P.; Jess, A. Deep desulfurization of oil refinery streams by extraction with ionic liquids. *Green Chem.* **2004**, *6*, 316. (b) Gasoline Sulfur. Gasoline Standards; U.S. Environmental Protection Agency , https://www.epa.gov/gasoline-standards/gasoline-sulfur.

(5) Turaga, U. T.; Song, C. S. MCM-41-supported Co-Mo Catalysts for Deep Hydrodesulfurization of Light Cycle Oil. *Catal. Today* **2003**, *86*, 129−140.

(6) (a) Sato, K.; Hyodo, M.; Aoki, M.; Zheng, X. Q.; Noyori, R. Oxidation of Sulfides to Sulfoxides and Sulfones with 30% Hydrogen Peroxide Under Organic Solvent- and Halogen-Free Conditions. *Tetrahedron* **2001**, *57*, 2469−2476. (b) Hu, Y. W.; He, Q. H.; Zhang, Z.; Ding, N. D.; Hu, B. W. Oxidative Desulfurization of Dithiobenzothiphene with Hydrogen Peroxide catalyzed by Selenium-(IV)-Containing Peroxotungstate. *Chem. Commun.* **2011**, *47*, 12194−12196. (c) Maurya, M. R.; Arya, A.; Kumar, A.; Kuznetsov, M. L.; Avecilla, F.; Pessoa, J. C. Polymer-bound Oxidovanadium(IV) and Dioxovanadium(V) Complexes as Catalysts for the Oxidative Desulfurization of Model Fuel Diesel. *Inorg. Chem.* **2010**, *49*, 6586−6600. (d) Zhu, W.; Li, H.; Jiang, X.; Yan, Y.; Lu, J.; Xia, J. Oxidative Desulfurization of Fuels Catalyzed by Peroxotungsten and Peroxomolybdenum Complexes in Ionic Liquids. *Energy Fuels* **2007**, *21*, 2514−2516. (e) Ramos-Luna, M. A.; Cedeno-Caero, L. Effect of Sulfates and Reduced-Vanadium Species on Oxidative Desulfurization (ODS) with V_2O_5/TiO_2 Catalysts. *Ind. Eng. Chem. Res.* **2011**, *50*, 2641−2649.

(7) (a) Kong, L.; Li, G.; Wang, X. Mild Oxidation of Thiophene over TS-1/H_2O_2. *Catal. Today* **2004**, *93*−*95*, 341−345. (b) Chica, A.; Corma, A.; Dómine, M. A. Catalytic Oxidative Desulfurization (ODS) of Diesel Fuel on a Continuous Fixed-bed Reactor. *J. Catal.* **2006**, *242*, 299−308.

(8) Thompson, D. J.; Cao, Z.; Judkins, E. C.; Fanwick, P. E.; Ren, T. Peroxo-dimolybdate catalyst for the oxygenation of organic sulfides by hydrogen peroxide. *Inorg. Chim. Acta* **2015**, *437*, 103−109.

(9) Wang, J.; Niu, Y.; Zhang, M.; Ma, P.; Zhang, C.; Niu, J.; Wang, J. Organophosphonate-Functionalized Lanthanopolyoxomolybdate: Synthesis, Characterization, Magnetism, Luminescence, and Catalysis of H_2O_2-Based Thioether Oxidation. *Inorg. Chem.* **2018**, *57*, 1796−1805.

(10) Ye, J.-X.; Wang, J.-Y.; Wang, X.; Zhou, M.-D. Alkylimidazolium/alkylpyridinium octamolybdates catalyzed oxidation of sulfides to sulfoxides/sulfones with hydrogen peroxide. *Catal. Commun.* **2016**, *81*, 1−3.

(11) Jacobson, S. E.; Tang, R.; Mares, F. Group 6 Transition Metal Peroxo Complexes Stabilized by Polydentate Pyridinecarboxylate Ligands. *Inorg. Chem.* **1978**, *17*, 3055−3063.

(12) Melman, A.; Lev, O.; Jenny, G.; Shelkov, R.; Ekeltchik, I. Bis(hydroxyamino)triazines: Versatile and High-affinity tridentate Hydroxylamine Ligands for Selective iron(III) chelation. *Dalton Trans.* **2006**, *10*, 1285−1293.

(13) Kabanos, T. A.; Nikolakis, V. A.; Chilas, G. I.; Jakusch, T.; Vaimakis, T.; Kiss, T.; Sigalas, M. P.; Keramidas, A. D.; Stylianou, M. "Molybdenum(VI) Coordination Chemistry of the N,N- Disubstituted Bis(hydroxylamido)-1,3,5-triazine ligand, H_2bihyat. Water-assisted Activation of the Mo^{VI}=O Bond and Reversible Dimerization of *cis*-[$Mo^{VI}O_2$(bihyat) to [$Mo_2{}^{VI}O_4$(bihyat)$_2$(H_2O)$_2$]. *Inorg. Chem.* **2012**, *51*, 13138−13147.

(14) Hadjithoma, S.; Papanikolaou, M. G.; Leontidis, E.; Kabanos, T. A.; Keramidas, A. D. Bis(hydroxylamino)triazines: High Selectivity and Hydrolytic Stability of Hydroxylamine-based Ligands for Uranyl Compared to Vanadium(V) and Iron(III). *Inorg. Chem.* **2018**, *57*, 7631−7643.

(15) Ivanov, A. S.; Parker, B. F.; Zhang, Z.; Aguila, B.; Sun, Q.; Ma, S.; Jansone-Popova, S.; Arnold, J.; Mayes, R. T.; Dai, S.; Bryantsev, V. S.; Rao, L.; Popovs, I. Siderophore-inspired Chelator Hijacks Uranium from Aqueous Medium. *Nat. Commun.* **2019**, *10*, No. 819.
(16) Bissing, D. E.; Matuszak, C. A.; McEwen, W. E. The mechanism of the acid-catalyzed rearrangement of triarylmethyl hydroperoxides. *J. Am. Chem. Soc.* **1964**, *86*, 3824−3828.
(17) Frisch, M. J.; Trucks, G. W.; Schlegel, H. B.; Scuseria, G. E.; Robb, M. A.; Cheeseman, J. R.; Scalmani, G.; Barone, V.; Petersson, G. A.; Nakatsuji, H.; Li, X.; Caricato, M.; Marenich, A. V.; Bloino, J.; Janesko, B. G.; Gomperts, R.; Mennucci, B.; Hratchian, H. P.; Ortiz, J. V.; Izmaylov, A. F.; Sonnenberg, J. L.; Williams-Young, D.; Ding, F.; Lipparini, F.; Egidi, F.; Goings, J.; Peng, B.; Petrone, A.; Henderson, T.; Ranasinghe, D.; Zakrzewski, V. G.; Gao, J.; Rega, N.; Zheng, G.; Liang, W.; Hada, M.; Ehara, M.; Toyota, K.; Fukuda, R.; Hasegawa, J.; Ishida, M.; Nakajima, T.; Honda, Y.; Kitao, O.; Nakai, H.; Vreven, T.; Throssell, K.; Montgomery, J. A., Jr.; Peralta, J. E.; Ogliaro, F.; Bearpark, M. J.; Heyd, J. J.; Brothers, E. N.; Kudin, K. N.; Staroverov, V. N.; Keith, T. A.; Kobayashi, R.; Normand, J.; Raghavachari, K.; Rendell, A. P.; Burant, J. C.; Iyengar, S. S.; Tomasi, J.; Cossi, M.; Millam, J. M.; Klene, M.; Adamo, C.; Cammi, R.; Ochterski, J. W.; Martin, R. L.; Morokuma, K.; Farkas, O.; Foresman, J. B.; Fox, D. J. *Gaussian 16*, Revision C.01; Gaussian, Inc.: Wallingford CT, 2016.
(18) Dennington, R.; Keith, T. A.; Millam, J. M. *GaussView*, version 6; Semichem Inc.: Shawnee Mission, KS, 2016.
(19) Legault, C. Y. *CYLView, 1.0b*; Université de Sherbrooke: Canada, 2009.
(20) (a) Becke, A. D. Density Functional Thermochemistry. III. The Role of Exact Exchange. *J. Chem. Phys.* **1993**, *98*, 5648−5652. (b) Lee, C.; Yang, W.; Parr, R. G. Development of the Colle-Salvetti Correlation- Energy Formula into a Functional of the Electron Density. *Phys. Rev. B* **1988**, *37*, 785−789.
(21) Weigend, F.; Ahlrichs, R. Balanced Basis Sets of Split Valence, Triple Zeta Valence and Quadruple Zeta Valence Quality for H to Rn: Design and Assessment of Accuracy. *Phys. Chem. Chem. Phys.* **2005**, *7*, 3297−3305.
(22) Grimme, S.; Antony, J.; Ehrlich, S.; Krieg, H. A consistent and accurate ab initio parameterization of density functional dispersion correction (DFT-D) for the 94 elements H-Pu. *J. Chem. Phys.* **2010**, *132*, No. 154104.
(23) Peng, C.; Schlegel, H. B. Combining Synchronous Transit and Quasi-Newton Methods for Finding Transition States. *Isr. J. Chem.* **1993**, *33*, 449−454.
(24) Mammen, M.; Shakhnovich, E. I.; Deutch, J. M.; Whitesides, G. M. Estimating the Entropic Cost of Self-Assembly of Multiparticle Hydrogen-Bonded Aggregates Based on the Cyanuric Acid·Melamine Lattice. *J. Org. Chem.* **1998**, *63*, 3821−3830.
(25) Martin, R. L.; Hay, P. J.; Pratt, L. R. Hydrolysis of Ferric Ion in Water and Conformational Equilibrium. *J. Phys. Chem. A* **1998**, *102*, 3565−3573.
(26) (a) Sieffert, N.; Bühl, M. Noncovalent Interactions in a Transition-Metal Triphenylphosphine Complex: a Density Functional Case Study. *Inorg. Chem.* **2009**, *48*, 4622−4624. (b) Li, H.; Wen, M.; Wang, Z.-X. Computational Mechanistic Study of the Hydrogenation of Carbonate to Methanol Catalyzed by the Ru^{II}PNN Complex. *Inorg. Chem.* **2012**, *51*, 5716−5727. (c) Qu, S.; Dang, Y.; Song, C.; Wen, M.; Huang, K.−W.; Wang, Z.−X. Catalytic Mechanisms of Direct Pyrrole Synthesis via Dehydrogenative Coupling Mediated by PNP-Ir or PNN-Ru Pincer Complexes: Crucial Role of Proton-Transfer Shuttles in the PNP-Ir System. *J. Am. Chem. Soc.* **2014**, *136*, 4974−4991. (d) Chen, P.-P.; Lucas, E. L.; Greene, M. A.; Zhang, S.-Q.; Tollefson, E. J.; Erickson, L. W.; Taylor, B. L. H.; Jarvo, E. R.; Hong, X. A Unified Explanation for Chemoselectivity and Stereospecificity of Ni-Catalyzed Kumada and Cross-Electrophile Coupling Reactions of Benzylic Ethers: A Combined Computational and Experimental Study. *J. Am. Chem. Soc.* **2019**, *141*, 5835−5855.
(27) Johnson, R. D., III *NIST Computational Chemistry Comparison and Benchmark Database*, NIST Standard Reference Database Number 101, Release 21, http://cccbdb.nist.gov/ (accessed 01-10-2020).
(28) (a) Scott, A. P.; Radom, L. Harmonic Vibrational Frequencies: An Evaluation of Hartree−Fock, Møller−Plesset, Quadratic Configuration Interaction, Density Functional Theory, and Semiempirical Scale Factors. *J. Phys. Chem. A* **1996**, *100*, 16502−16513. (b) Sinha, P.; Boesch, S. E.; Gu, C.; Wheeler, R. A.; Wilson, A. K. Harmonic Vibrational Frequencies: Scaling Factors for HF, B3LYP, and MP2 Methods in Combination with Correlation Consistent Basis Sets. *J. Phys. Chem. A* **2004**, *108*, 9213−9217. (c) Assefa, M. K.; Devera, J. L.; Brathwaite, A. D.; Mosleya, J. D.; Duncan, M. A. Vibrational Scaling Factors for Transition Metal Carbonyls. *Chem. Phys. Lett.* **2015**, *640*, 175−179.
(29) (a) Bagherzadeh, M.; Haghdoost, M. M.; Amini, M.; Derakhshandeh, P. G. Molybdenum oxo-peroxo complex: A very Fast Catalyst for Oxidation and Reduction of Sulfur-based Compounds. *Catal. Commun.* **2012**, *23*, 14−19. (b) Amini, M.; Bagherzadeh, M.; Atabaki, B.; Derakhshandeh, P. G.; Ellern, A.; Woo, K. Molybdenum(VI)-oxodiperoxo Complex Containing an Oxazine Ligand: Synthesis, X-ray studies, and Catalytic activity. *J. Coord. Chem.* **2014**, *67*, 1429−1436.
(30) Sanz, R.; Pedrosa, M. R. Applications of Dioxomolybenum(VI) Complexes in Organic Synthesis. *Curr. Org. Synth.* **2009**, *6*, 239−263.
(31) Von Felten, H.; Wernli, B.; Gamsjäger, H.; Baertschi, P. Oxygen Exchange Between Oxo- anions and Water in Basic Media Molybdate(2-) and Tungstate(2-). *J. Chem. Soc., Dalton Trans.* **1978**, 496−500.
(32) Que, L. *Physical Methods in Bioinorganic Chemistry*; University Science Books: Sausalito CA, 2000.
(33) Mimoun, H. The role of Peroxymetallation in Selective Oxidative Processes. *J. Mol. Catal.* **1980**, *7*, 1−29.
(34) Chong, A. O.; Sharpless, K. B. Epoxidation of olefins by alkyl hydroperoxides. *J. Org. Chem.* **1977**, *42*, 1587−1590.
(35) (a) Bagherzadeh, M.; Amini, M. Synthesis, Characterization and Catalytic Study of a Novel iron(III)-tridentate Schiff base Complex in Sulfide Oxidation by UHP. *Inorg. Chem. Commun.* **2009**, *12*, 21−25. (b) Varma, R. S.; Naicker, K. P. The urea-hydrogen peroxide complex: solid-state oxidative protocols for hydroxylated aldehydes and ketones (Dakin reaction), nitriles, sulfides, and nitrogen heterocycles. *Org. Lett.* **1999**, *1*, 189−191.
(36) Gould, S. J.; Kirchmeier, M. J.; LaFever, R. E. Incorporation of two oxygens from $^{18}O_2$ in the epoxyquinone from dihydroxyacetanilide epoxidase reaction: evidence for a dioxygenase mechanism. *J. Am. Chem. Soc.* **1996**, *118*, 7663−7666.
(37) Kuo, L. Y.; Perera, N. M. Paraoxon and parathion hydrolysis by aqueous molybdocene dichloride (Cp_2MoCl_2): First reported pesticide hydrolysis by an organometallic complex. *Inorg. Chem.* **2000**, *39*, 2103−2106.
(38) Baig, N.; Madduluri, V. K.; Sha, A. K. Selective Oxidation of Organic Sulfides to Sulfoxides Using Sugar Derived *cis*-Dioxo Molybdenum(VI) Complexes: Kinetic and Mechanistic Studies. *RSC Adv.* **2016**, *6*, 28015−28022.
(39) Bagherzadeh, M.; Tahsini, L.; Latifi, R.; Woo, K. *Cis*-Dioxomolybdenum(VI)-oxazoline complex catalyzed epoxidation of olefins by *tert*-butyl hydrogen peroxide. *Inorg. Chim. Acta* **2009**, *362*, 3698−3702.
(40) (a) Valente, A. A.; Moreira, J.; Lopes, A. D.; Pillinger, M.; Nunes, C. D.; Romão, C. C.; Kühn, F. E.; Gonçalves, I. S. Dichloro and dimethyl dioxomolybdenum(VI)-diazabutadiene complexes as catalysts for the epoxidation of olefins. *New J. Chem.* **2004**, *28*, 308. (b) Kühn, F. E.; Groarke, M.; Bencze, E.; Herdtweck, E.; Prazeres, A.; Santos, A. M.; Calhorda, M. J.; Ramão, C. C.; Gonçalves, I. S.; Lopes, A. D.; Pillinger, M. Octahedral Bipyridine and Bipyrmidine Dioxomolybdenum(VI) Complexes: Characterization, Application in Catalytic Epoxidation, and Density Functional Mechanistic Study. *Chem. - Eur. J.* **2002**, *8*, 2370−2383. (c) Veiros, L. F.; Prazeres, A.; Costa, P. J.; Ramão, C. C.; Kühn, F. E.; Calhorda, M. J. Olefin Epoxidation with *tert*-Butyl Hydroperoxide Catalyzed by MoO_2X_2L

https://doi.org/10.1021/acs.inorgchem.1c00145
Inorg. Chem. 2021, 60, 7762−7772

Complexes: a DFT Mechanistic Study. *Dalton Trans.* **2006**, 1383−1389.
(41) Veiros, L. F.; Gamelas, C. A.; Calhorda, M. J.; Ramão, C. C. Chemoselective Sulfide and Sulfoxide Oxidations by $CpMo(CO)_3Cl$/HOOR: a DFT Mechanistic Study. *Organometallics* **2011**, *30*, 1454−1465.
(42) (a) Carey, F. A.; Sundberg, R. J. *Advanced Organic Chemistry: Structure and Mechanisms*; Kluwer Academic: New York, 2007; pp 179−191. (b) Breno, K. L.; Tyler, D. R. C−H Bond Activation in Aqueous Solution: A Linear Free Energy Relationship Investigation of the Rate-Limiting Step in the H/D Exchange of Alcohols Catalyzed by a Molybdocene. *Organometallics* **2001**, *20*, 3864−3868.
(43) Kamata, K.; Hirano, R.; Ishimoto, N.; Mizuno, N. Sulfoxidation with Hydrogen Peroxide Catalyzed by $[SeO_4\{WO(O_2)_2\}_2]^{2-}$. *Dalton Trans.* **2010**, *39*, 5509−5518.
(44) (a) Bortolini, O.; Campestrini, S.; Di Furia, F.; Modena, S.; Valle, G. Metal catalysis in Oxidation by Peroxides. Anionic molybdenum-picolinate N-oxido-peroxo Complex: an Effective Oxidant of Primary and Secondary Alcohols in Nonpolar Solvents. *J. Org. Chem.* **1987**, *52*, 5467−5469. (b) Campestrini, S.; Conte, V.; Di Furia, F.; Modena, G.; Bortolini, O. Metal catalysis in oxidation by peroxides. 30. Electrophilic oxygen transfer from anionic, coordinatively saturated molybdenum peroxo complexes. *J. Org. Chem.* **1988**, *53*, 5721−5724.
(45) Oyerinde, O. F.; Weeks, C. L.; Anbar, A. D.; Spiro, T. G. Solution structure of molybdic acid from Raman spectroscopy and DFT analysis. *Inorg. Chim. Acta* **2008**, *361*, 1000−1007.

https://doi.org/10.1021/acs.inorgchem.1c00145
Inorg. Chem. 2021, 60, 7762−7772